Photoemission and STM Study of the Morphology and Electronic Structure of Benz[a]anthracene on Cu(111) on Mica and on HOPG

ARTICLE *in* THE JOURNAL OF PHYSICAL CHEMISTRY C · MARCH 2011

Impact Factor: 4.77 · DOI: 10.1021/jp111975n

2 AUTHORS:

Kedar Manandhar
University of Illinois at Chicago
20 PUBLICATIONS **90** CITATIONS
SEE PROFILE

Bruce A Parkinson
University of Wyoming
251 PUBLICATIONS **7,087** CITATIONS
SEE PROFILE

THE JOURNAL OF PHYSICAL CHEMISTRY C

ARTICLE

pubs.acs.org/JPCC

Photoemission and STM Study of the Morphology and Electronic Structure of Benz[a]anthracene on Cu(111) on Mica and on HOPG

K. Manandhar and B. A. Parkinson*

Department of Chemistry, School of Energy Resources, University of Wyoming, Laramie, Wyoming 82071, United States

ABSTRACT: The interfacial electronic structure of benz[a]anthracene (BA) films on the Cu(111) on mica surface and on HOPG in ultrahigh vacuum are studied using X-ray and ultraviolet photoelectron spectroscopy (XPS and UPS) and the surface structure is studied with scanning tunneling microscopy (STM). Large energy level shifts are measured during the deposition of the first 6 Å of a BA film after which no significant band movements are measured. A Schottky junction formed between BA and copper consisted of a 0.21 eV interface dipole with a hole barrier height of 1.78 eV. Room temperature STM investigation of a near monolayer coverage of BA revealed a very interesting honeycomb structural motif. An arrangement of the BA molecules consistent with the STM data is presented and discussed.

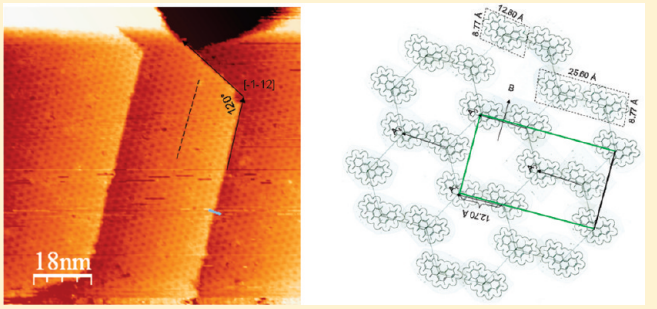

I. INTRODUCTION

Organic molecules exhibiting semiconductor and optoelectronic properties are of interest for their application in large area and low-cost electronics and opto-electronics such as full color flat panel displays, lighting panels, and large area photovoltaic cells.[1−3] These devices include organic thin film transistors (OTFTs), photovoltaic (PV) cells, and organic light emitting diodes (OLEDs), all of which have recently demonstrated improved performance.[4−8] The molecules in these devices are deposited as thin films of a few nanometers to several nanometers in thickness that can conveniently be manufactured at ambient temperature using a printing and/or roll-to-roll processes,[9−11] enabling the production of low cost large area devices.

The interfaces within a few nanometers of the active layers in thin film devices influence the electronic and optical properties of the organic film and the device performance.[12−17] Therefore, from the technological point of view, understanding and controlling organic/metal interfaces is of tremendous importance. Investigation of the electronic properties of many organic−metal interfaces revealed barrier properties ranging from the Schottky limit to the Bardeen limit.[18−20] The initial assumption was that the organic/metal interfaces will follow the Schottky limit because the weak van der Waals interactions would not produce interface states that would pin the Fermi level. In spite of extensive research, the physics behind the electronic structure of these interfaces is still not well understood and requires more systematic investigations of the relationship between the work function of the contacting metal, the highest occupied molecular orbital (HOMO), the lowest unoccupied molecular orbital (LUMO) levels of the molecule as well as the orientation and delocalization of the electronic states of the molecule on the formation and magnitude of interfacial dipoles and barriers.

Another important aspect of organic/electrode interfaces is the arrangement of the molecules. The ordering within the first layer is especially important for templating the growth of the thicker film, which in turn influences the electronic structure of the interface as well as the charge transport across the interface. Recently, it has been shown that the ordering and orientation of the organic molecules is crucial for the device efficiency by demonstrating that device characteristics are influenced by the anisotropy of the transport properties in the film.[21] Thus, a detailed understanding of the adsorption of the first layer of molecules on metal surface, which often forms interesting surface structures and packing motifs, is of prime importance.

Benz[a]anthracene (BA) (insert in part a of Figure 1) is a planar polyaromatic hydrocarbon molecule comprised of four fused benzene rings and is chiral when confined to a plane surface. To our knowledge, the interfacial electronic properties and thin film structure of BA molecule on metal surfaces has not yet been investigated. However, tetracene, which is an isomer of BA, has exhibited very good field effect mobility for holes of 0.1 $cm^2/(V\ s)$.[22,23] The investigation of the other chiral isomer chrysene on Cu/mica by our group has shown that thin films of this molecule show a classical Stranski−Krastanov (SK) film growth mode with measured hole barrier height of 1.8 eV and interface dipole potential of 0.8 eV.[19] The study of the another 2D chiral molecule naphtho[2,3-a]pyrene (NP) on Au(111) also revealed a SK type growth mode with interface dipole potential of 0.99 eV and hole barrier height of 0.6 eV.[24] The STM investigation of nominal 1 ML NP showed at least two different structural

Received: December 16, 2010
Revised: February 23, 2011
Published: March 14, 2011

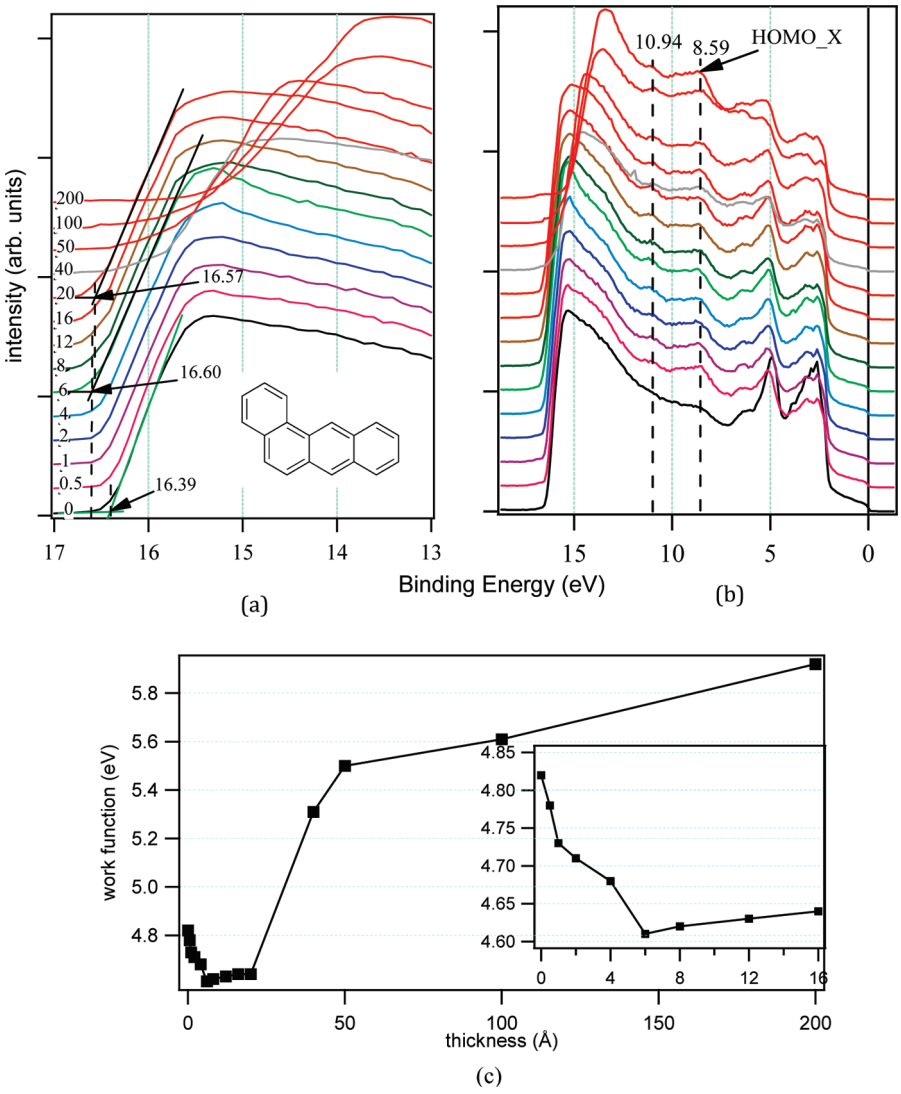

Figure 1. UPS He I spectra of BA film onto Cu(111). (a) high binding energy cutoff (HBEC) region and the insert is the molecular structure of benz[a]anthracene (BA). (b) full spectra. (c) A plot of work function of Cu(111) versus BA thickness. The insert is the plot for BA thickness up to 16 Å.

polytypes. The first polytype had domains comprised of a single 2D enantiomeric form of NP with uniform packing of the NP molecules. A second structure is a paired row type containing homochiral pairs.

In this contribution, we have utilized X-ray photoelectron (XPS), UV photoelectron spectroscopy (UPS), and UV−vis spectroscopies to investigate the BA/Cu interface electronic structure and film growth mode. Scanning tunneling microscope (STM) has been used to image the structures formed at nominal 1 ML coverages of BA. The nominal 1 ML is roughly equal to 1.0 ± 0.2 ML as measured by quartz crystal microbalance (QCM).

II. EXPERIMENTAL SECTION

Experiments were performed in a commercial Omicron Multiprobe ultrahigh vacuum (UHV) system (base pressure 8 × 10^{-10} Torr). This system is equipped with a variable temperature STM (VT-STM) for surface structural characterization. XPS and UPS, using a VSW EA125 single channel hemispherical analyzer, were used to study the electronic structure of the interface. A physical vapor deposition chamber (base pressure 1 × 10^{-8} Torr) is attached to the UHV system allowing samples and films to be prepared in situ.

The copper films were prepared in the load lock of the vacuum chamber by evaporating copper onto freshly cleaved mica. The micas were outgassed overnight at around 410 °C and held at temperature at around 250 °C during copper evaporation. The deposition rate, as monitored by quartz crystal growth monitor, was about 260 Å/min. The copper film was approximately 1500 Å thick. Cycles of sputtering at 1 keV energy with Ar-partial pressure of 7 × 10^{-7} Torr and annealing at 400 °C were used to clean and flatten the copper surface. The chemical purity of the surface was determined with XPS (Mg kα, 50 eV pass energy) and the presence of flat surfaces was confirmed with STM.[25] The surfaces revealed terraces as large as 1 μm × 1 μm with monatomic step heights 1.90 Å, which is within 8% error from the accepted values of 2.08 Å. In small area scanning, the hexagonal structure of the lattice was with the measured lattice constants of 2.30 Å, which are within 10% error from the accepted 2.56 Å.

Benz[a]anthracene (BA) (Aldrich Chemical Co.) films were deposited under UHV (base pressure 1 × 10^{-8} Torr) using a

silicone rubber flexible heater to resistively heat a quartz ampule prepared from a UHV series quartz-metal adapter (source temperature ~110 °C). The source was extensively degassed at about 100 °C prior to deposition. The quartz ampule containing BA was heated to obtain a desired deposition rate that was monitored by a Leybold quartz crystal microbalance (QCM). The deposition rate was on average 1.5 ML/min with 1 ML is defined as a thickness of 6 Å as measured by the QCM. The Cu/mica substrates were maintained at room temperature (RT) during the deposition.

Sequential depositions were performed onto copper substrates up to a final film thickness of 200 Å. After each growth step, XPS and UPS (HeI, 21.21 eV; with 10 eV pass energy) were utilized to measure the electronic structure of the surface. XPS spectra were taken with a takeoff angle of ~20° from the normal emission, whereas UPS spectra were collected under normal emission. A −10.00 V bias was applied to the sample for the UPS measurements to separate the sample and spectrometer high binding energy cutoffs (HBECs). The spectrometer was calibrated as previously described.[26] Work function and HOMO-cutoff positions were determined from the HBECs and HOMO onsets respectively of UP spectra. XPS core level peak positions were determined by fitting routine using IGOR Pro (Wavemetrics) data evaluation software. A vacuum deposited BA film (film thick enough to be able to notice characteristic molecular color) on quartz was used to obtain the thin film solid-state absorption spectrum that was measured using a Varian Cary−500 UV−vis−NIR spectrophotometer.

III. RESULTS AND DISCUSSION

Interface Dipole. The orbital energy alignment between copper and BA was measured utilizing both UPS and XPS. A clean Cu/mica sample was prepared and characterized and BA was then deposited in fourteen steps to a final thickness of 200 Å. The HBEC region and complete He I UPS spectra as a function of BA deposition are presented in parts a and b of Figure 1, respectively. Changes in the band structure are evident as the BA film thickness increases. The existence of a large interface dipole is suggested by the significant shift in the HBEC (part a of Figure 1) between the bare copper sample and the 6 Å thick BA film. The work function of the copper substrate was determined by subtracting the HBEC of the bare copper UP spectra from the source energy (21.21 eV) yielding Φ = 4.82 eV. This work function is slightly smaller than the published value of 4.98 eV for single crystal Cu(111),[27,28] however a copper film on mica contains other copper orientations. On the basis of the prevalent multiterraced flat surfaces as large as 490 × 490 nm imaged with STM scans of 800 × 800 nm and the hexagonal lattice structure observed in atomic resolution scans as well as the sharp hexagonal spots in LEED, we estimate that more than 60% of the surface of the copper film has a (111) orientation. The work function of the film after deposition of 6 Å of BA was determined to be 4.61 eV. For the BA thickness of up to 20 Å, the WF of the copper is constant within ±0.03 eV. However the WF gradually increases at higher thicknesses. This change in WF with no change in HOMO_X position (discussed below), implies a change in the ionization potential of the molecular film. This change in WF may originate from a change in the BA orientation.[20,29,30] The shift in the work function as a function of BA film thickness is plotted in part c of Figure 1. The magnitude of interface dipole is associated with the dipole layer formed right at the interface.[31] As there was no band bending measured (discussed later), the total work function shift of 0.21 eV calculated from the difference between the bare surface and the 6 Å deposition step represents the magnitude of the interface dipole formed by BA on Cu/mica.

Film Growth Mode. Part a and b of Figure 2 are plots of C1s and Cu2p intensity as a function of binding energy (BE). The C1s spectra in part a of Figure 2 show that initially the C1s (BE), associated with a small amount of carbon contamination on the copper surface, is 284.70 eV (part a of Figure 2).[31,32] For the initial sub-ML BA deposition, the BE gradually reduces to 284.53 eV at 6 Å thickness and remains within 0.05 eV of this value up to a thickness of 200 Å. Part c of Figure 2 shows the normalized C1s and $Cu2p_{3/2}$ intensities as a function of the BA coverage on the copper substrate. The decrease in $Cu2p_{3/2}$ and increase in C1s intensity was most significant when the BA thickness was 6 Å (insert in part c of Figure 2). The C1s intensity was 19% of its eventual maximum whereas the Cu2p was 76% of its initial value (part c of Figure 2). The noticeable changes in intensities of the core level emissions at 6 Å of BA, the constant BE of the C1s core level emission starting at 6 Å, and the significant change of the copper work function between the bare copper and 6 Å of BA (insert in part c of Figure 1) indicate that at around 6 Å the copper is uniformly covered with BA. There is a decrease in the rate of change of photoemission intensities at intermediate coverages (part c of Figure 2). The Cu2p signal is still discernible after deposition of 200 Å of BA (part c of Figure 2). Additionally in the UPS spectra of the 200 Å thick BA, a Fermi step and 3d valence band state features related to the Cu substrate are observable (part b of Figure 1). This is most likely due to the formation of BA islands.[33] We therefore conclude that for the deposition conditions given above, the growth mode for BA on Cu/mica follows the Stranski−Krastanov (SK) growth where an initial wetting layer is followed by island growth.

Band Bending and Band Diagram. The He I UPS spectra in part b of Figure 1 show that subsequent depositions of the aromatic molecule results in the photoemission from the valence states of copper being gradually suppressed by the spectrum of the organic film. The evolution of the HOMO levels of BA in the UPS spectra on Cu/mica is very difficult to evaluate (part b of Figure 1) as the emission from the valence band region and the Cu3d states overlap in energy with the increasing emission from HOMO levels of BA.[19] Fortunately, in the BE region between 8 and 11.5 eV there are no prominent copper states and upon deposition of BA new strong BA emissions are visible (labeled HOMO_X in part b of Figure 1) at 8.59 eV ± 0.20 and 10.90 eV ± 0.20 eV. The photoemission features of HOMO_X do not change with increasing film thickness (part b of Figure 1).

Band bending occurring in the organic material, or polarization energy-related shifts at the interface, was determined by the measurement of shifts in the core level photoemission peaks. The Cu2p peaks are not subject to any band bending-related shifts and the $Cu2p_{3/2}$ peak is constant at 932.60 eV after all deposition steps (part b of Figure 2).[19,20] As previously discussed, there were no shifts in the C1s core level BE related to BA deposition. The constant BEs of the BA emissions in UPS corroborate the C1s core level XPS results, providing no evidence for band bending in the BA films.

The energy difference between the copper Fermi level and the HOMO-cutoff of BA is of interest because it represents the height of the hole injection barrier (E_{bh}). However, as explained above, it is very difficult to evaluate the HOMO levels of BA

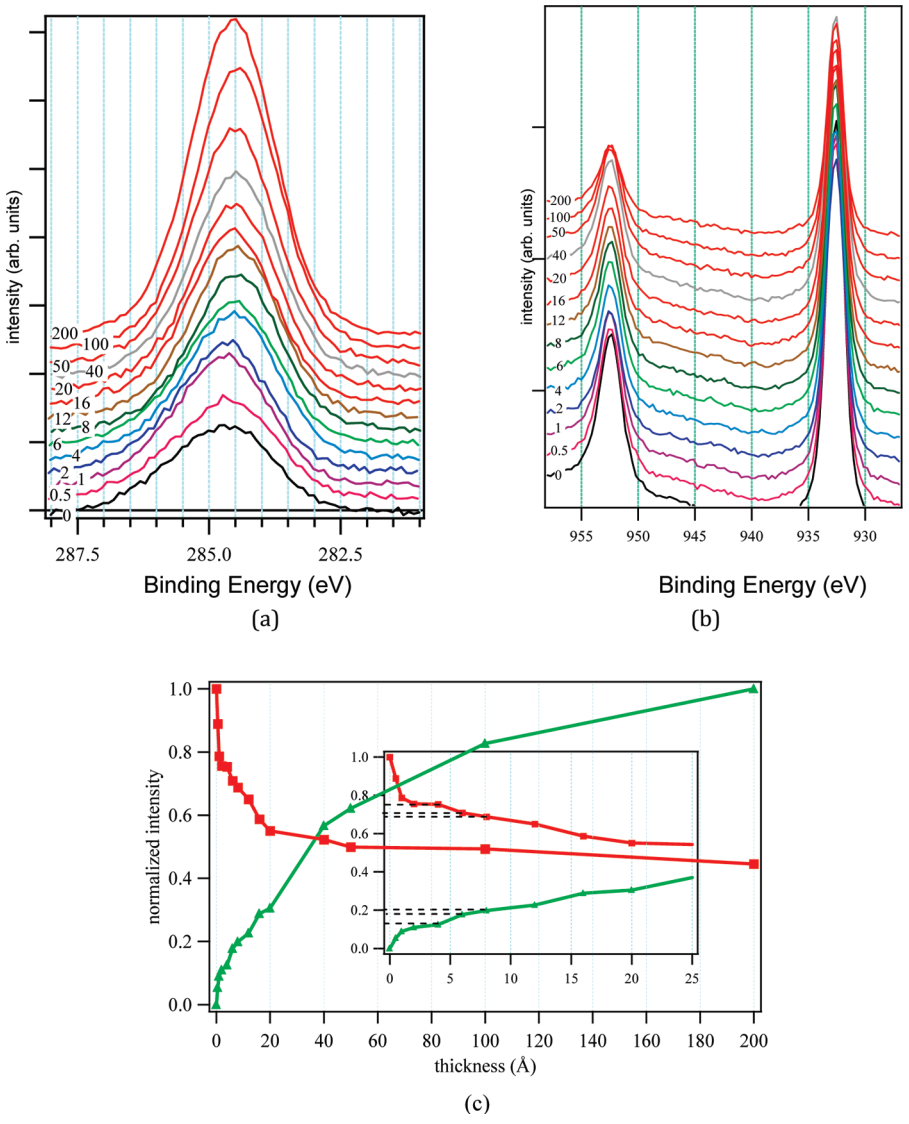

Figure 2. (a) and (b) are C1s and Cu2p XPS spectra of 0−200 Å thick BA, respectively; (c) a plot of normalized intensity of C1s (green curve with filled triangle) and Cu2p (red curve with filled square) versus BA thickness. The insert is an expanded scale plot for BA thicknesses up to 25 Å.

because of overlap of copper 3d valence band states with BA HOMO levels. The absence of strong emissions from HOPG in the binding energy range below 11 eV (part a of Figure 3) enables the determination of the HOMO cutoff position for BA. The characteristic featureless UPS spectrum of bare HOPG below 11 eV is given in part a of Figure 3.[34,35] Immediately after the first BA deposition step (part a of Figure 3), a number of new emissions appear that grow only slightly after the initial deposition step and exhibit no shape change for films up to 200 Å thick. A close examination of the photoemission onset allows for the determination of the HOMO cutoff position at a binding energy of 1.74 eV (part b of Figure 3). The other HOMO labeled HOMO_X in figure is at 8.55 ± 0.04 eV (part b of Figure 3). The difference between the first HOMO_X emission and the HOMO cutoff is 6.81 eV (part b of Figure 3). This difference is a material property of BA molecule and is constant[19,36] and is used to calculate the HOMO-cutoff position of the BA films on the copper substrate. In the experiment with BA/Cu/mica, BA assigned HOMO states are visible and these are also labeled as HOMO_X (part b of Figure 1) as in the spectra collected on HOPG. The HOMO-cutoff of the BA spectra for BA/Cu/mica is HOMO_X BE of BA/Cu/mica minus 6.81 eV and is calculated to be 1.78 eV representing E_{bh}, the offset between copper Fermi level and the HOMO-cutoff of the BA.

The position of the LUMO cannot be measured directly with XPS or UPS, however the BA band gap can be estimated using the onset energy of optical absorption of a thin solid-state film of BA. The visible absorption spectrum of a solid-state BA thin film evaporated onto a quartz slide is shown in part a of Figure 4. The lowest energy absorption maximum occurs at 474.0 nm, corresponding to the first excitonic transition at 2.60 eV. (It is important to note that the first excitionic transition is only used as an estimate for the HOMO−LUMO gap since the large excitonic BE of the molecules is not accounted for and results in an overestimate of the actual band gap.[24])

The estimated band gap (E_{bg}) for BA allows for the determination of the energy level position of the BA LUMO states with respect to the copper Fermi level by subtracting E_{bg} (2.60 eV)

dx.doi.org/10.1021/jp111975n |J. Phys. Chem. C 2011, 115, 5910–5918

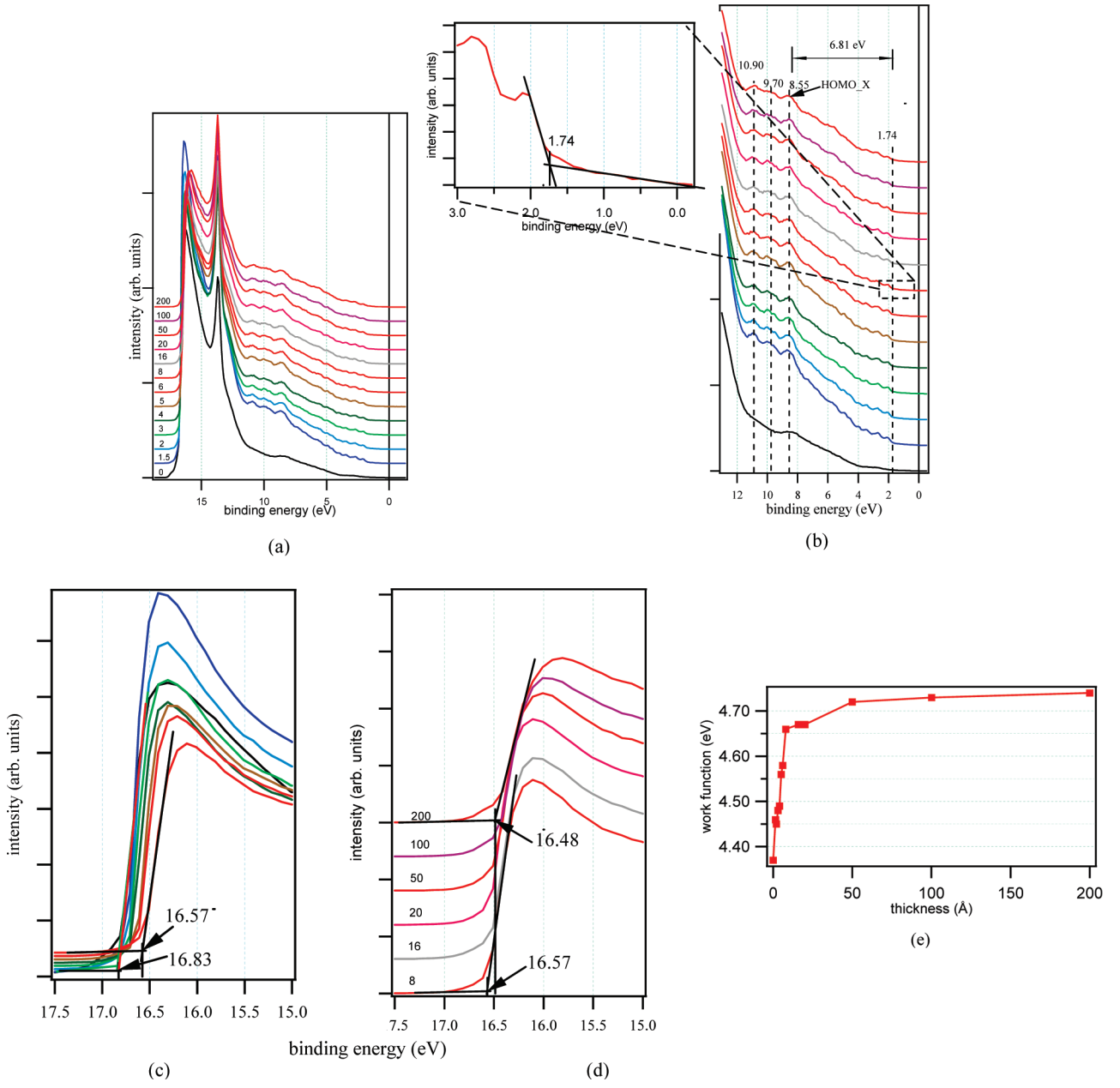

Figure 3. UPS He I spectra of BA film deposited on HOPG. (a) full spectra (b) BA spectra range consisting of HOMO_X. Zoomed in view of HOMO cutoff region of 8 Å thick BA film (c) high binding energy cutoff (HBEC) region of 0 to 8 Å thick film. (d) high binding energy cutoff (HBEC) region of 8 to 200 Å thick film. (e) a plot of work function of HOPG versus BA thickness.

from E_{bh} (1.78 eV). This analysis yields the magnitude of the electron injection barrier for electrons to be injected into the organic material at the interface (E_{be} = 0.82 eV). The ionization energy (IE) of BA was determined by adding the work function of the 6 Å BA film (4.61 eV) to the HOMO cutoff (1.78 eV) of the same spectra, yielding 6.39 eV. This value is smaller by 1.02 eV than the IE of bulk BA 7.41 eV[38] experimentally determined from photoelectron spectra using He I. This is consistent with the IE in a condensed film being less by about 1.2 eV than in the bulk phase for most organic molecules.[39] This decrease in the IE in a condensed film is attributed to electronic polarization of the surrounding film in the solid state which screens the hole resulting from the removal of an electron from a single molecule.[39] All of these energy values result in an estimate of the band line up for BA on Cu/mica since these measurements do not include the polarization related shifts. This information is graphically summarized in the energy alignment diagram of part b of Figure 4.

From the experimental UPS spectrum data described above, the BA on HOPG electronic properties can be summarized in a band energy diagram given in part c of Figure 4. The bare HOPG UPS spectrum shows the well-known strong graphitic carbon related feature between 13 and 14 eV (part a of Figure 3). During the BA deposition, the work function changed from 4.38 eV for the bare HOPG to 4.64 eV for 8 Å thick BA film is as shown in parts c and e of Figure 3. The HBEC remain constant within ±0.03 eV for BA thickness from 8 Å to 20 Å indicating no apparent change in the work function of HOPG (part e of

dx.doi.org/10.1021/jp111975n |J. Phys. Chem. C 2011, 115, 5910–5918

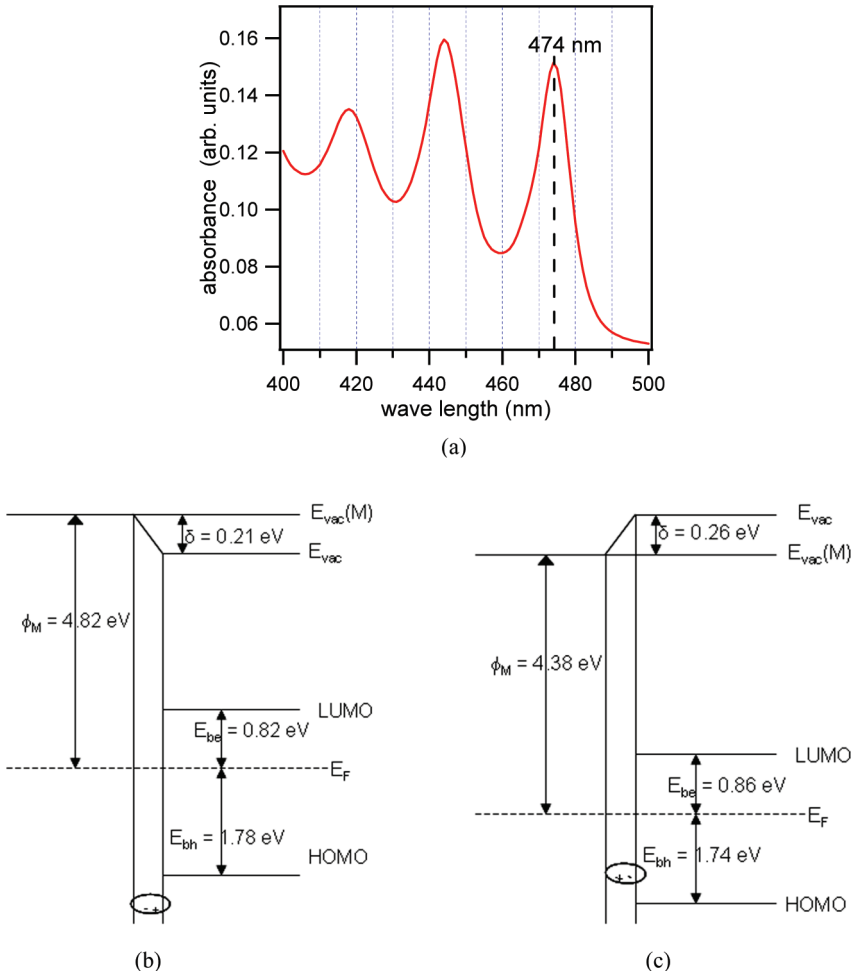

Figure 4. (a) Visible absorption spectrum of BA; (b) the band diagram of BA-Cu(111) showing the interface dipole; (c) the band diagram of BA-HOPG showing the interface dipole.

Figure 3). However, after 20 Å, the BE of HBEC gradually reduces again producing gradual increase in apparent work function of HOPG (parts d and e of Figure 3), leading to work function of 4.73 eV for 200 Å BA. In agreement with the other substrates, no binding energy shifts in HOMO emissions were observed during the deposition of BA on HOPG (part b of Figure 3), so no band bending is present in films on HOPG. With no band bending, the 0.26 eV difference in work functions between that of bare HOPG and the HOPG with about 8 Å thick BA, at which the substrate is predicted entirely covered with BA, directly translates into the interface dipole potential of δ = 0.26 eV. The interface dipole is directed from HOPG (part c of Figure 4) into molecule, opposite to the direction from the molecules into copper in the BA/Cu/mica (part b of Figure 4) system, representing a partial charge transfer from HOPG into BA. The LUMO-cutoff position was again estimated by applying the UV−vis determined optical band gap (part a of Figure 4) and the electron injection barrier E_{be} = 0.86 and the IP = 6.38 eV are calculated as explained above for BA/Cu/mica.

Morphology-Dependent BA Features. Despite the fact that the binding energies and the energy splittings are similar on copper and HOPG substrates, the full spectra reveal some differences in BA photoemission features (part b of Figure 1, and part b of Figure 3). The features in BA/Cu/mica spectra are broader than those in BA/HOPG spectra. The BA features at 8.59 ± 0.04 eV and 10.87 ± 0.04 eV are discerned immediately after the first deposition (part b of Figure 1, and part b of Figure 3) in both BA/cu/mica and BA/HOPG. In addition to the two peaks, a peak at 9.70 ± 0.03 eV in the spectrum of the film formed after the first deposition on HOPG is observed (part b of Figure 3). This peak is not observed in the BA spectra of BA/Cu/mica as it is concealed by the broadened two peaks at 10.94 and 8.59 eV (part b of Figure 1). STM images of the bare substrates showed the HOPG is atomically flat and the copper surface is predominately made up of flat islands with a small fraction of a "rolling hill" morphology. Adsorbed molecules will be more randomly oriented on the "rolling hills" (STM images not shown) with respect to the surface normal. A photoemission peak represents a statistical average value of photoemission from the molecules with different orientations and with varying interactions with neighboring molecules in the layer.[19,37,40] Therefore, the different shapes of the photoemission spectra for molecular films on copper and HOPG may be attributed to differences in the average orientation of the molecules. This has been well documented by detailed photoelectron spectroscopy studies of pentacene and other PAH molecules on different substrates.[19,20,32] It is noteworthy that studies of nominal 1 ML coverages of similar PAHs on gold, silver and copper by our group have reported many different 2D lattice structures.[32,33] Therefore, the different 2D lattice structures with differing

dx.doi.org/10.1021/jp111975n |J. Phys. Chem. C 2011, 115, 5910–5918

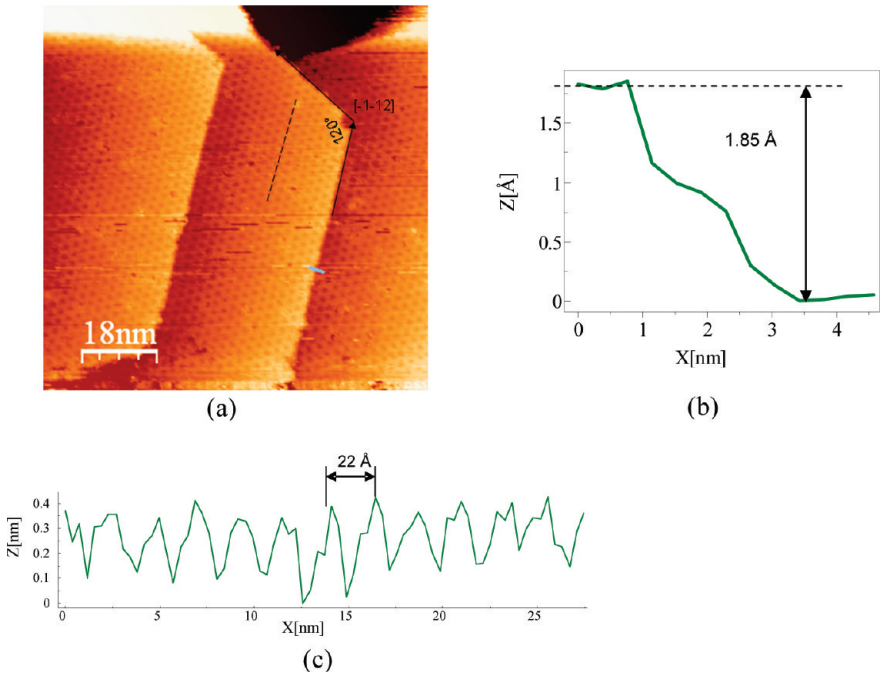

Figure 5. (a) STM images of nominal 1 ML BA film on Cu(111) (92 × 92 nm, −2.0 V, 1.1 nA). (b) the line profile along the light blue line across the step in (a). (c) the line profile along the dotted line in (a).

molecule−molecule interactions on the flat terraces of copper and HOPG may also influence the different shapes of the emission peaks.

STM Imaging of BA Surface. Only noisy STM images were obtained at sub-ML BA coverages due to the molecular motion at RT being faster than the time scale of the STM imaging process as is the case with many PAH molecules on metal surfaces near RT,[32,33,41−44] whereas BA-molecules self-organize into 2D crystalline overlayers near ML coverages (part a of Figure 5). For near ML BA films on Cu(111), large area scans (as large as 92 × 92 nm) show that the entire surface has ordered 2D overlayer. Part a of Figure 5 shows a 92 × 92 nm area STM image with a terraced surfaces covered with a BA overlayer structure. Part b of Figure 5 shows a height profile along the line across the step in part a of Figure 5. The measured step height is 1.85 Å, which is within experimental error of the accepted monatomic step height of 2.08 Å for Cu(111).[32] The angle between the step edges of a terrace is 120° ± 1° (part a of Figure 5) as expected for a hexagonal symmetry surface. It is well-known that the majority of step edges on (111) noble metal surfaces run along the close packed direction [-1-12].[43,45,46] The direction of step edges thus represent the [-1-12] direction of the Cu(111) surface. A direction of the dotted line in part a of Figure 5, which is the line B in part a of Figure 6, is along the direction of step edges (part a of Figure 5) [-1-12] of the Cu(111) crystallographic direction.

Part a of Figure 6 is a higher magnification STM image of the overlayer which shows a regular repetition of a honeycomb pattern enclosing a ∼13 Å diameter hole (part c of Figure 6) at the center (dotted circle in part a of Figure 6). The two sides of a honeycomb hexagon are formed from the regular repetition of thick and long high topography features (represented with dotted lines A1, A2, A3 and A4 in part a of Figure 6). The high topographies in the STM image represent BA molecules. Line profiles along A (part d of Figure 6) and B (part c of Figure 6) show that the high topography features are 29.0 ± 2.0 Å long and 9.0 ± 1.5 Å wide, respectively. 9.0 ± 1.5 Å corresponds to the vdW width of the single BA molecule (part e of Figure 6). Considering tip interference on molecules along scanning direction and the other experimental errors, the 29.0 ± 2.0 Å corresponds to the vdW length of BA arranged as shown in the model (part e of Figure 6). A possible model of BA molecules' organization in the hexagon creating a hole at the center is shown in part e of Figure 6. The surface structure results 38.1 ± 1.5 × 21.8 ± 1.5 Å rectangular lattice with four molecules per unit cell (rectangle formed of green dotted line in part e of Figure 6.

At nominal 1 ML, a large group of achiral PAH without heteroatoms forms close-packed 2D molecular monolayer on (111) noble metal surfaces and hydrogen passivated Si(001).[32,33,47,48] Also, a chiral PAH without heteroatom such as naphtho[2,3-*a*]pyrene (NP) and chrysene on the gold surface formed close-packed homochiral domains at nominal 1 ML.[24,49] It is interesting that BA, however, forms a honeycomb pattern with large void of ∼13 Å diameter at the center. We attribute the formation of this pattern to a long-range surface-state mediated repulsive interaction.[50−52] This effect was explained by standing waves in the surface state free electron gas.[51] Repp et al. measured that the nodes of such oscillatory nature surface state electron density, which correspond to the minima of interaction energy for Cu adatoms on Cu(111), were at 12.5, 27, 41.5, and 57 Å.[51] Cu adatoms find stable position at these nodes with the possible closest adatoms distance of 12.5 Å. For pentacene on Cu(110), the adsorbate separation was measured to be 28 ± 2 Å[50] and it was 52 ± 2 Å for anthraquinone on Cu(1111)[52] for coverages from sub-ML to close to 1 ML. The number 28 ± 2 Å and 52 ± 2 Å agree within experimental error with the measured minima positions of 27 and 57 Å for Cu adatoms on Cu(111). It is worth mentioning that the Cu adatoms form islands with a local hexagonal structure and that anthraquinone molecules also form an extended honeycomb pattern on the Cu(111) substrate, however pentacene on Cu(110) form 1D molecular rows. The

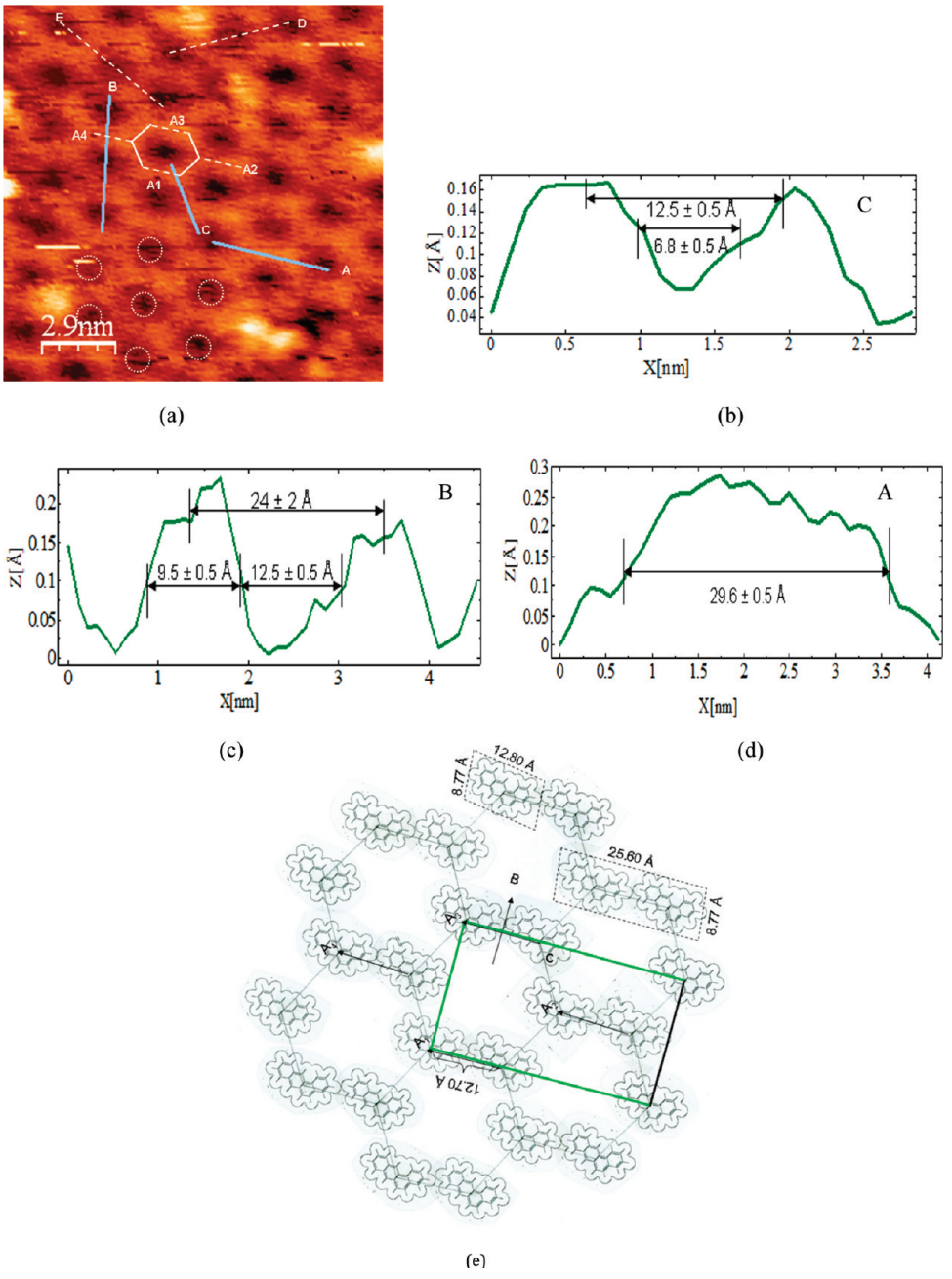

Figure 6. (a) High-resolution STM image (14.8 × 14.8 nm, −2.1 V, 0.5 nA) of nominal 1 ML film onto Cu(111). (b) the line profile along the light blue line C in (a). (c) the line profile along the light blue line B in (a). (d) the line profile along the light blue line A in (a). (e) a model showing possible structure of BA lattice in (a). Rectangle formed of green lines is the overlayer unit lattice. The dotted parallelogram represent 2D vdW dimension of the monomer and dimer BA. The arrows A_1 to A_4 represent line A_1 to A_4 in (a) and the line C represents the line C in (a).

Fermi surface of the surface state in Cu(111) is almost circular allowing for standing waves running along all of the surface directions,[50] whereas the surface state in Cu(110) is located at $\bar{Y}$ point[53] (Figure 3 in ref 53), so that the standing waves for that surface should run along only one direction.[50] We therefore attribute the honeycomb overlayer motifs formed of BA molecules to the almost circular electron standing waves running along all surface directions. The measurement of the distances of ~24 ± 2 Å (part c of Figure 6) between the centers of the molecules in the hexagon agree well within the experimental error with the measured node position of 27 Å as mentioned above.

CONCLUSIONS

We investigated thin films of benz[a]anthracene (BA) grown on copper/mica using UPS, XPS and STM. The constant binding energy of C1s core level emissions in XPS and BA emissions in UPS provided no evidence of band bending in BA/copper/mica. The evolution of the HOMO levels of BA in the UPS spectra on copper is very difficult to evaluate as the valence band region the Cu3d states of copper overlap with the growing HOMO levels of BA. The HOMO position was determined based on the observed HOMO_X at 8.59 eV of BA/Cu(111) and the difference of HOMO_X and the HOMO cutoff of BA/HOPG. The band line

dx.doi.org/10.1021/jp111975n |J. Phys. Chem. C 2011, 115, 5910–5918

up of BA on copper illustrated that a Schottky barrier is formed between these materials with electron and hole injection barriers of 0.82 and 1.78 eV, respectively. An interface dipole of 0.21 eV was measured for the 6 Å BA covered interface. The UPS and XPS spectra indicated that at approximately 6 Å thickness a wetting layer of BA was formed followed by island growth. Under RT conditions, no ordered domains were observed for sub-ML coverages presumably due to the highly mobile nature of the BA molecules. For the nominal 1 ML coverages, the film exhibited a honeycomb pattern with a one molecule long diameter hole in the center. A speculative molecular arrangement for the honeycomb structure is presented. The formation of this open structure is believed to be related to a surface-state mediated repulsive interaction.

AUTHOR INFORMATION

Corresponding Author

*E-mail: bparkin1@uwyo.edu, tel: +1 307 766 4363, fax: +1 307 766 2807.

ACKNOWLEDGMENT

This work was supported by NSF Grant No. CHE-0518563 and University of Wyoming startup funds.

REFERENCES

(1) Tal, O.; Gao, W.; Chan, C. K.; Kahn, A.; Rosenwaks, Y. *Appl. Phys. Lett.* **2004**, *85*, 4148.
(2) Scharber, M. C.; Wuhlbacher, D.; Koppe, M.; Denk, P.; Waldauf, C.; Heeger, A. J.; Brabec, C. L. *Adv. Mater.* **2006**, *18*, 789.
(3) Harrop, P.; Das, R. *Organic Electronics Forecasts*, Players & Opportunities 2005−2025; ID techEx, 2006.
(4) Tang, C. W.; Vanslyke, S. A. *Appl. Phys. Lett.* **1987**, *51*, 913.
(5) Shen, C.; Kahn, A.; Hill, I. G. *Conjugated Polymer and Molecular Interfaces*; Marcel Dekker: New York.
(6) Gundlach, D. J.; Lin, Y. Y.; Jackson, T. N.; Nelson, S. F.; Schlom, D. G. *IEEE Electron Device Lett.* **1997**, *18*, 87.
(7) Lin, L. B.; Jenekhe, S. A.; Young, R. H.; Borsenberger, P. M. *Appl. Phys. Lett.* **1997**, *70*, 2052.
(8) Lin, Y. Y.; Gundlach, D. J.; Nelson, S. F.; Jackson, T. N. *IEEE Electron Device Lett.* **1997**, *18*, 606.
(9) Loo, Y. L.; Someya, T.; Baldwin, K. W.; Bao, Z. N.; Ho, P.; Dodabalapur, A.; Katz, H. E.; Rogers, J. A. *Proc. Natl. Acad. Sci. U.S.A.* **2002**, *99*, 10252.
(10) McCulloch, I. *Nat. Mater.* **2005**, *4*, 583.
(11) Rogers, J. A.; Bao, Z.; Baldwin, K.; Dodabalapur, A.; Crone, B.; Raju, V. R.; Kuck, V.; Katz, H.; Amundson, K.; Ewing, J.; Drzaic, P. *Proc. Natl. Acad. Sci. U.S.A.* **2001**, *98*, 4835.
(12) Park, Y. D.; Lim, J. A.; Lee, H. S.; Cho, K. *Mater. Today* **2007**, *10*, 46.
(13) Wang, S. D.; Kanai, K.; Ouchi, Y.; Seki, K. *Org. Electron.* **2006**, *7*, 457.
(14) Walzer, K.; Maennig, B.; Pfeiffer, M.; Leo, K. *Chem. Rev.* **2007**, *107*, 1233.
(15) Mitschke, U.; Bauerle, P. *J. Mater. Chem.* **2000**, *10*, 1471.
(16) Pfeiffer, M.; Leo, K.; Zhou, X.; Huang, J. S.; Hofmann, M.; Werner, A.; Blochwitz-Nimoth, J. *Org. Electron.* **2003**, *4*, 89.
(17) Schneider, M.; Umbach, E.; Sokolowski, M. *Chem. Phys.* **2006**, *325*, 185.
(18) Hill, I. G.; Rajagopal, A.; Kahn, A.; Hu, Y. *Appl. Phys. Lett.* **1998**, *73*, 662.
(19) Jaeckel, B.; Sambur, J.; Parkinson, B. A. *J. Phys. Chem. C* **2009**, *113*, 1837.
(20) Jaeckel, B.; Sambur, J. B.; Parkinson, B. A. *J. Appl. Phys.* **2008**, *103*, 063719.
(21) Ostrick, J. R.; Dodabalapur, A.; Torsi, L.; Lovinger, A. J.; Kwock, E. W.; Miller, T. M.; Galvin, M.; Berggren, M.; Katz, H. E. *J. Appl. Phys.* **1997**, *81*, 6804.
(22) Gundlach, D. J.; Nichols, J. A.; Zhou, L.; Jackson, T. N. *Appl. Phys. Lett.* **2002**, *80*, 2925.
(23) Lim, S. H.; Bjorklund, T. G.; Spano, F. C.; Bardeen, C. J. *Phys. Rev. Lett.* **2004**, 92.
(24) France, C. B.; Parkinson, B. A. *Langmuir* **2004**, *20*, 2713.
(25) Barth, J. V.; Brune, H.; Ertl, G.; Behm, R. J. *Phys. Rev. B* **1990**, *42*, 9307.
(26) Schroeder, P. G.; France, C. B.; Park, J. B.; Parkinson, B. A. *J. Phys. Chem. B* **2003**, *107*, 2253.
(27) Cardona, M., Ley, L. *Photoemission in Solids*; Springer-Verlag: Berlin, 1978, 1979; Vols. 1 and 2.
(28) Holzl, J. a. S., F., K. *Work Function of Metals in Solid Surface Physics*; Springer-Verlag: Berlin, 1979.
(29) Duhm, S.; Heimel, G.; Salzmann, I.; Glowatzki, H.; Johnson, R. L.; Vollmer, A.; Rabe, J. P.; Koch, N. *Nat. Mater.* **2008**, *7*, 326.
(30) Koch, N.; Vollmer, A.; Duhm, S.; Sakamoto, Y.; Suzuki, T. *Adv. Mater.* **2007**, *19*, 112.
(31) Ishii, H.; Sugiyama, K.; Ito, E.; Seki, K. *Adv. Mater.* **1999**, *11*, 605.
(32) Manandhar, K.; Parkinson, B. A. *J. Phys. Chem. C* **2010**, *114*, 14394.
(33) Manandhar, K.; Sambur, J. B.; Parkinson, B. A. *J. Appl. Phys.* **2010**, 107.
(34) Ruiz, R.; Choudhary, D.; Nickel, B.; Toccoli, T.; Chang, K. C.; Mayer, A. C.; Clancy, P.; Blakely, J. M.; Headrick, R. L.; Iannotta, S.; Malliaras, G. G. *Chem. Mater.* **2004**, *16*, 4497.
(35) Schroeder, P. G.; France, C. B.; Parkinson, B. A.; Schlaf, R. *J. Appl. Phys.* **2002**, *91*, 9095.
(36) Schroeder, P. G.; Nelson, M. W.; Parkinson, B. A.; Schlaf, R. *Surf. Sci.* **2000**, *459*, 349.
(37) Amy, F.; Chan, C.; Kahn, A. *Org. Electron.* **2005**, *6*, 85.
(38) Boschi, R.; Clar, E.; Schmidt, W. *J. Chem. Phys.* **1974**, *60*, 4406.
(39) Hill, I. G.; Makinen, A. J.; Kafafi, Z. H. *J. Appl. Phys.* **2000**, *88*, 889.
(40) Krause, S.; Casu, M. B.; Scholl, A.; Umbach, E. *New J. Phys.* **2008**, 10.
(41) Manandhar, K.; Ellis, T.; Park, K. T.; Cai, T.; Song, Z.; Hrbek, J. *Surf. Sci.* **2007**, *601*, 3623.
(42) Manandhar, K.; Park, K. T.; Ma, S.; Hrbek, J. *Surf. Sci.* **2009**, *603*, 636.
(43) Chizhov, I.; Scoles, G.; Kahn, A. *Langmuir* **2000**, *16*, 4358.
(44) Lackinger, M.; Hietschold, M. *Surf. Sci.* **2002**, *520*, L619.
(45) Dumont, J.; Wiame, F.; Ghijsen, J.; Sporken, R. *Surf. Sci.* **2004**, *572*, 459.
(46) Baski, A. A.; Fuchs, H. *Surf. Sci.* **1994**, *313*, 275.
(47) Tersigni, A.; Shi, J.; Jiang, D. T.; Qin, X. R. *Phys. Rev. B* **2006**, *74*, 205326.
(48) France, C. B.; Schroeder, P. G.; Parkinson, B. A. *Nano Lett.* **2002**, *2*, 693.
(49) France, C. B.; Parkinson, B. A. *J. Am. Chem. Soc.* **2003**, *125*, 12712.
(50) Lukas, S.; Witte, G.; Woll, C. *Phys. Rev. Lett.* **2002**, 88.
(51) Repp, J.; Moresco, F.; Meyer, G.; Rieder, K. H.; Hyldgaard, P.; Persson, M. *Phys. Rev. Lett.* **2000**, *85*, 2981.
(52) Pawin, G.; Wong, K. L.; Kwon, K. Y.; Bartels, L. *Science* **2006**, *313*, 961.
(53) Heimann, P.; Hermanson, J.; Miosga, H.; Neddermeyer, H. *Sur. Sci.* **1979**, *85*, 263.